

Reliable Majority Vote Computation with Complementary Sequences for UAV Waypoint Flight Control

Alphan Şahin, *Member, IEEE* and Xiaofeng Wang, *Member, IEEE*

Abstract—In this study, we propose a non-coherent over-the-air computation scheme to calculate the majority vote (MV) reliably in fading channels. The proposed approach relies on modulating the amplitude of the elements of complementary sequences based on the sign of the parameters to be aggregated. Since it does not use channel state information at the nodes, it is compatible with time-varying channels. To demonstrate the efficacy of our method, we employ it in a scenario where an unmanned aerial vehicle is guided by distributed sensors, relying on the MV computed using our proposed scheme. We show that the proposed scheme notably reduces the computation error rate with a longer sequence length in fading channels while maintaining the peak-to-mean-envelope power ratio of the transmitted orthogonal frequency division multiplexing signals to be less than or equal to 3 dB.

Index Terms—Complementary sequences, OFDM, over-the-air computation, power amplifier non-linearity.

I. INTRODUCTION

Multi-user interference is often considered an undesired phenomenon for communication systems as it can degrade the link performance. In contrast, the same underlying phenomenon, i.e., the signal superposition property of wireless multiple-access channels, can be very useful in the computation of special mathematical functions by harnessing the additive nature of the wireless channel. The gain obtained with over-the-air computation (OAC) is that the resource usage can be reduced to a one-time cost, which otherwise scales with the number of devices [2]–[4]. Hence, OAC can benefit applications by reducing the latency when a large number of nodes participate in computation over limited resources. Nevertheless, the transmitted signals for OAC are perturbed by noise and distorted by fading and hardware impairments such as power amplifier (PA) non-linearity and synchronization errors. To address these issues, in this work, we propose a non-coherent OAC method for majority vote (MV) computation with complementary sequences (CSs) [5]. We demonstrate its efficacy for an unmanned aerial vehicle (UAV) waypoint flight control scenario, where a UAV is guided by many distributed sensors harnessing the multi-user interference to use the limited wireless resources as efficiently as possible.

Alphan Şahin and Xiaofeng Wang are with the Electrical Engineering Department, University of South Carolina, Columbia, SC, USA. E-mail: asahin@mailbox.sc.edu, wangxi@cec.sc.edu

This paper was presented in part at the IEEE Military Communications Conference 2023 [1].

A. Related Work and Challenges

1) *Over-the-air computation*: The idea of function computation over a multiple-access channel (MAC) was first thoroughly analyzed in Bobak’s pioneering work in [6]. In [7] and [8], Goldenbaum shows that OAC can be utilized to compute a family of functions, i.e., nomographic functions, including arithmetic mean, norm, polynomial function, maximum, and MV. OAC has recently gained momentum with an increased number of applications where the ultimate purpose of communications is computation. For example, the authors in [9]–[12] implement federated learning (FL) [13] over a wireless network, where OAC is used for aggregating a large number of gradients or model parameters of the edge devices at an edge server efficiently. Similarly, OAC is considered for split learning in [14] to aggregate smashed data, i.e., the outputs of a neural network. We refer the readers to [2]–[4], [15], and [16] and the references therein for OAC and its exciting applications, such as distributed localization, wireless data centers, and wireless control systems.

The primary challenge of computing functions via signal superposition is that the receiver observes the superposition of the signals *distorted* by the wireless channels between the receiver and transmitters. To address this issue, a large number of studies adopt pre-equalization techniques, where the parameters desired to be aggregated are distorted with the reciprocals of the channel coefficients before the transmission so that a coherent superposition is achieved at the receiver [11], [12], [17], [18]. This approach can provide excellent results when the phase synchronization among the devices can be maintained. Furthermore, as the effective channel corresponds to an additive white Gaussian noise (AWGN) channel, the reliability of OAC can be improved further with lattice codes [6], [8], [19], [20]. However, in practice, it is very difficult to maintain the phase synchronization as the phase response of the *composite* wireless channel (i.e., including the responses of the transmitter and receiver) is a strong function of mobility and hardware impairments such as clock errors, residual carrier frequency offset (CFO), and time-synchronization errors. For instance, a single sample deviation can cause large phase rotations in the frequency domain [21] and only a ± 15 -degree phase mismatch across the transmitters can degrade the OAC performance dramatically [20, Fig. 4]. In [22], it is shown that non-stationary channel conditions in a UAV network can severely deteriorate the coherent signal superposition. In [23] and [24], a more

practical scheme where the transmitters are blind (i.e., no channel state information (CSI) at the transmitters) while the receiver has an estimate of the aggregated CSI (i.e., the sum of fading coefficients across the links) is considered. It is shown that using a large number of antennas at the receiver can mitigate the interference components arising due to the inner product operation to estimate the superposed values. However, this approach may not be viable when the computing node has limited space and battery life. To overcome the phase synchronization bottleneck, another approach is to use non-coherent OAC at the expense of sacrificing more resources. For instance, two orthogonal resources are allocated to compute an MV function in [10] and [25] by exploiting the energy accumulation via modulation techniques such as frequency-shift keying (FSK), pulse-position modulation (PPM), and chirp-shift keying (CSK). In [26], the authors demonstrate this approach in practice by using five Adalm Pluto software-defined radios (SDRs) to train a neural network without phase synchronization across the transmitters. Similarly, in [27], orthogonal resources are used for negative- and positive-valued aggregation with FSK and CSK. By using more resources along with a decomposition relying on a balanced number system, a quantized OAC is investigated in [28]. The aforementioned non-coherent techniques exploit type-function, i.e., frequency histogram, by defining discrete classes to compute functions such as arithmetic mean, maximum, minimum, and median [29], [30]. In [31] and [32], random unimodular sequences are proposed to be utilized at the devices. In this method, a transmitter modulates the energy of the sequence with the parameter to be aggregated. At the receiver, the energy of the received superposed sequence is calculated for continuous-valued OAC at the expense of interference components. A proof of concept demonstration regarding Goldenbaum's approach is provided in [33]. Nevertheless, achieving reliable computation with a non-coherent OAC technique in a fading channel is still an unsolved issue in the literature.

The second challenge for reliable computation arises because the received signal powers of the nodes need to be similar, if not identical. If a transmitted signal for OAC has a large peak-to-mean envelope power ratio (PMEPR), it can result in a reduced cell size due to the power back-off or a higher adjacent channel interference due to the PA saturation [25]. The adjacent channel interference can also increase further due to the simultaneous transmissions from many nodes participating in OAC. In the literature, few OAC schemes are analyzed from the perspective of PMEPR. To reduce PMEPR, chirps and single-carrier (SC) waveforms are used in [25] and [34], respectively. It is well-known that the PMEPR of the orthogonal frequency division multiplexing (OFDM) signals using CSs is less than or equal to 3 dB while achieving some coding gain [35]. However, to the best of our knowledge, CSs have not been utilized for reliable OAC while reducing the dynamic range of the transmitted OFDM signals.

2) *Wireless Control Systems*: Suppose a control unit needs to receive feedback from a larger number of sensors over wireless links for a control application. In this scenario, without OAC, orthogonal wireless resources must be allocated

to the sensors to receive sensory data, and the control unit must wait for the acquisition to be completed to perform the desired computation. As a result, the latency (or resource consumption) increases linearly with the number of sensors, which can cause an unstable system response or a slower system. To address this issue, the stability of a dynamic plant is investigated under limited wireless resources in [34], and OAC is exploited to compute the feedback from a large number of distributed sensors as quickly as possible to ensure the stability of a dynamic plant. In [36], a general state-space model of a discrete-time linear time-invariant system is proposed to be computed with OAC. In [37], OAC is utilized to achieve mean consensus for a vehicle platooning application. It is shown that all vehicles converge to a specific value proportional to the average position without using an orthogonal multiplexing technique. With the same motivation for reducing the latency, in this work, we consider a scenario where a UAV receives feedback from distributed erroneous sensors to infer its flying direction as quickly as possible so that it can fly stably. To our knowledge, the UAV waypoint flight control scenario has not been investigated in the literature by taking OAC into account. It is also worth mentioning that OAC is investigated in specific scenarios that involve UAVs. For instance, in [38], the UAVs compute the arithmetic mean of ground sensor readings with OAC. In [39], UAV trajectories are optimized based on the locations of the sensors. However, the purpose of OAC is not wireless control in these papers.

B. Contributions

In this study, we focus on computing MVs reliably in fading channels. Our contributions can be listed as follows:

- We propose a new non-coherent OAC scheme based on CSs [40] to improve the robustness of computation against fading channels while limiting the dynamic range of transmitted signals to mitigate the distortion due to hardware non-linearity. Since the proposed approach does not rely on the availability of CSI at the transmitters and receiver, it also provides robustness against time-varying channels and time-synchronization errors.
- By extending our preliminary work in [1], we rigorously analyze the computation error rate (CER) of the proposed OAC scheme. We derive the CER in Corollary 2 and Corollary 3 based on Lemma 2.
- We demonstrate the applicability of the proposed method to a UAV flight control scenario based on MV computation. We provide the corresponding convergence analysis and show that the proposed approach is globally uniformly ultimately bounded in mean square in Theorem 3.
- We support our findings with comprehensive simulations. We also generate numerical results based on Goldenbaum's OAC scheme in [31] to provide a comparative analysis.

Organization: The rest of the paper is organized as follows. Section II provides the notation and preliminary discussions used in the rest of the sections. In Section III, the proposed OAC scheme is discussed in detail. In Section IV,

TABLE I
NOTATION SUMMARY.

Notation	Meaning of the notation
\mathbb{C}	The sets of complex numbers
\mathbb{R}	The sets of real numbers
\mathbb{Z}_H	The sets of integers modulo H
\mathbb{Z}_H^m	The set of m -dimensional integers where each element is in \mathbb{Z}_H
$\mathbb{E}[\cdot]$	The expectation of its argument over all random variables
$\mathcal{CN}(0, \sigma^2)$	A zero-mean symmetric complex Gaussian distribution with variance σ^2
$\mathcal{U}_{[a,b]}$	The uniform distribution with the support between a and b
$\Phi(\cdot)$	The cumulative distribution function (CDF) of the standard normal distribution
$F_x(a; b)$	The CDF of a random variable x evaluated at a for a given parameter b
$\varphi(t)$	The characteristic function of a random variable x , i.e., $\mathbb{E}[e^{jt x}]$
$\Pr(A; x)$	The probability of the event A with a parameter x
$\Pr(A B)$	The conditional probability of an event A given the event B
$\mathbf{1}_L$	A vector of length L , where its elements are only 1
$\mathbf{0}_L$	A vector of length L , where its elements are only 0
$(a_i)_{i=0}^{L-1}$	A sequence of length L , i.e., $\mathbf{a} = (a_0, a_1, \dots, a_{L-1})$
x^*	The complex conjugate of $x \in \mathbb{C}$
$\max\{a, b\}$	The maximum element of (a, b)
$\text{sign}(\cdot)$	The signum function
$\lfloor \cdot \rfloor$	The floor function
$\lceil \cdot \rceil$	The ceiling function
$f: \mathbb{Z}_2^m \rightarrow \mathbb{R}$	A pseudo-Boolean function
e	Euler's constant
j	$\sqrt{-1}$

we theoretically analyze the CER of the proposed scheme. In Section V, the convergence of the UAV waypoint flight control is discussed. In Section VI, we assess the proposed scheme numerically. We conclude the paper in Section VII. A summary of the notation used throughout the paper is given in TABLE I.

II. SYSTEM MODEL

Consider a scenario where a UAV flies from one point of interest $(c_{i,1}, c_{i,2}, c_{i,3})$ to another point of interest $(c_{t,1}, c_{t,2}, c_{t,3})$. Suppose that the UAV cannot localize its location in the room. However, it can receive feedback from $K \geq 1$ sensors¹ deployed in the room about the velocity of the UAV on the x -, y -, and z -axis for every T_{update} seconds. Based on the feedback from the sensors, the UAV updates its position at the ℓ th round for the x -, y -, and z -axis, denoted by $c_1^{(\ell)}$, $c_2^{(\ell)}$, and $c_3^{(\ell)}$, respectively, as

$$c_l^{(\ell+1)} = c_l^{(\ell)} - T_{\text{update}} u_l^{(\ell)}, \quad (1)$$

where

$$u_l^{(\ell)} = \begin{cases} \max\{\mu g_l^{(\ell)}, -u_{\text{limit}}\} & g_l^{(\ell)} < 0 \\ \min\{\mu g_l^{(\ell)}, u_{\text{limit}}\} & g_l^{(\ell)} \geq 0 \end{cases}, \quad (2)$$

for $c_i^{(0)} \triangleq c_{i,l}$, $\forall l \in \{1, 2, 3\}$. In (1) and (2), $u_l^{(\ell)}$ is the velocity at the ℓ th round for the l th coordinate, $u_{\text{limit}} > 0$ is

¹To localize the UAVs, the sensors can rely on computer vision techniques and use wide-angle cameras. For example, the sensor can exploit the changes in the features of the environment by comparing them with those previously created 3-D maps or use stereo vision capture and depth maps, as discussed in [41] and [42].

the maximum velocity of the UAV, $\mu > 0$ is the update rate, $g_l^{(\ell)}$ is the velocity-update strategy given by

$$g_l^{(\ell)} = \begin{cases} \frac{1}{K} \sum_{k=1}^K \tilde{c}_{k,l}^{(\ell)} - c_{t,l}, & \text{Cont. (ideal)} \\ \text{sign} \left(\underbrace{\sum_{k=1}^K \text{sign}(\tilde{c}_{k,l}^{(\ell)} - c_{t,l})}_{\triangleq \tilde{c}_{k,l}^{(\ell)}} \right), & \text{MV (ideal)} \\ \hat{w}_l^{(\ell)}, & \text{MV (OAC)} \end{cases}, \quad (3)$$

where $\tilde{c}_{k,l}^{(\ell)} = c_i^{(\ell)} + \epsilon_{k,l}^{(\ell)}$ is an estimate of the l th coordinate of the UAV position at the k th sensor, $\tilde{c}_{k,l}^{(\ell)}$ is the k th sensor's vote for the l th coordinate, $\epsilon_{k,l}^{(\ell)}$ is a zero-mean Gaussian variable with the variance σ_s^2 , and $w_l^{(\ell)}$ and $\hat{w}_l^{(\ell)}$ denote the MV computed under perfect communications and the MV obtained with the proposed scheme (i.e., (14)) for the l th coordinate, respectively. We use the term *ideal* to imply perfect communication between the sensors and the UAV.

In (3), the UAV averages the sensors' outputs to decide which direction to fly for the continuous case. In the MV cases, such averaging is not possible. Instead, the UAV goes in the direction (with the length $\pm \mu T_{\text{update}}$) on each coordinate based on the majority of the sensors' output. Note that an MV-based update was previously investigated in machine learning literature, showing that an MV-based update is related to an update based on the sign of the median value [43]. Finally, we note that the model can be more sophisticated than the one in (1) and take other dynamics, such as UAV imperfections, into account [44]. Since our paper focuses on OAC, we use (1) as a baseline control model to assess the proposed OAC scheme.

A. Complementary Sequences

Let $\mathbf{a} = (a_i)_{i=0}^{L-1} \triangleq (a_0, a_1, \dots, a_{L-1})$ be a sequence of length L for $a_i \in \mathbb{C}$ and $a_{L-1} \neq 0$. We associate the sequence \mathbf{a} with the polynomial $A(z) = a_{L-1}z^{L-1} + a_{L-2}z^{L-2} + \dots + a_0$ in indeterminate z . The aperiodic auto-correlation function (AACF) of the sequence \mathbf{a} given by

$$\rho_{\mathbf{a}}(k) \triangleq \begin{cases} \sum_{i=0}^{L-k-1} a_i^* a_{i+k}, & 0 \leq k \leq L-1 \\ \sum_{i=0}^{L+k-1} a_i a_{i-k}^*, & -L+1 \leq k < 0 \\ 0, & \text{otherwise} \end{cases}. \quad (4)$$

If $\rho_{\mathbf{a}}(k) + \rho_{\mathbf{b}}(k) = 0$ holds for $k \neq 0$, the sequences \mathbf{a} and \mathbf{b} are referred to as CSs [5]. It can be shown the PMEPR of an OFDM symbol constructed based on a CS is less than or equal to 3 dB [35].

Let $f(\mathbf{x})$ be a map from $\mathbb{Z}_2^m = \{\mathbf{x} \triangleq (x_1, x_2, \dots, x_m) | \forall x_j \in \mathbb{Z}_2\}$ to \mathbb{R} as $f: \mathbb{Z}_2^m \rightarrow \mathbb{R}$, i.e., a pseudo-Boolean function. A family of CSs can be obtained by using pseudo-Boolean functions as follows:

Theorem 1 ([40]). Let $\pi = (\pi_n)_{n=1}^m$ be a permutation of $\{1, 2, \dots, m\}$. For any $H, m \in \mathbb{Z}^+$, $a_n, a_0 \in \mathbb{R}$, and $b_n, b_0 \in \mathbb{Z}_H$ for $n \in \{1, 2, \dots, m\}$, let

$$f_r(\mathbf{x}) = \sum_{n=1}^m a_n y_{\pi_n} + a_0, \quad (5)$$

$$f_i(\mathbf{x}) = \frac{H}{2} \sum_{n=1}^{m-1} x_{\pi_n} x_{\pi_{n+1}} + \sum_{n=1}^m b_n x_{\pi_n} + b_0, \quad (6)$$

where y_{π_n} is $(x_{\pi_n} + x_{\pi_{n+1}})/2$ and x_{π_m} for $n < m$ and $n = m$, respectively. Then, the sequence $\mathbf{t} = (t_0, \dots, t_{L-1})$, where its associated polynomial is given by

$$T(z) = \sum_{\forall \mathbf{x} \in \mathbb{Z}_2^m} \underbrace{e^{f_r(\mathbf{x})} e^{j \frac{2\pi}{H} f_i(\mathbf{x})}}_{t_i(\mathbf{x})} z^{i(\mathbf{x})}, \quad (7)$$

is a CS of length $L = 2^m$, where $i(\mathbf{x}) \triangleq \sum_{j=1}^m x_j 2^{m-j}$, i.e., a decimal representation of the binary number constructed using all elements in the sequence \mathbf{x} .

Theorem 1 shows that the functions that determine the amplitude and the phase of the elements of the CS \mathbf{t} (i.e., $f_r(\mathbf{x})$ and $f_i(\mathbf{x})$) and Reed-Muller (RM) codes have similar structures. The function $f_i(\mathbf{x})$ is in the form of the cosets of the first-order RM code within the second-order RM code [35]. Notice that the mapping between $\{(y_1, \dots, y_m)\}$ and $\{(x_1, \dots, x_m)\}$ is bijective and results in a Gray code when the elements of the set $\{(x_1, \dots, x_m)\}$ are ordered lexicographically [40]. Hence, the function $f_r(\mathbf{x})$ is also similar to the first-order RM code, except that the operations occur in \mathbb{R} . We refer the readers to [45] for various representations of CSs and their properties.

B. Signal Model and Wireless Channel

We assume that the sensors and the UAV are equipped with a single antenna. Let $\mathbf{t}_k^{(\ell)} = (t_{k,0}^{(\ell)}, \dots, t_{k,L-1}^{(\ell)})$ be a CS of length L transmitted from the k th sensor over an OFDM symbol by mapping its elements to a set of contiguous subcarriers. Assuming that all sensors access the wireless channel simultaneously and the cyclic prefix (CP) duration is larger than the sum of the maximum time-synchronization error and the maximum-excess delay of the channel, we can express the polynomial representation of the received sequence $\mathbf{r}^{(\ell)} = (r_0^{(\ell)}, \dots, r_{L-1}^{(\ell)})$ at the UAV after the signal superposition as

$$R(z) = \sum_{i=0}^{L-1} \underbrace{\left(\sum_{k=1}^K h_{k,i} \sqrt{P_k} t_{k,i}^{(\ell)} + \omega_i \right)}_{r_i^{(\ell)}} z^i, \quad (8)$$

where $h_{k,i} \sim \mathcal{CN}(0, 1)$ is the Rayleigh fading channel coefficient between the UAV and the k th sensor for the i th element of the sequence unless otherwise stated, P_k is the average transmit power, and $\omega_i \sim \mathcal{CN}(0, \sigma_{\text{noise}}^2)$ is the AWGN.

We assume that the average received signal powers of the sensors at the UAV are aligned with a power control mechanism. This assumption is weak as the impact of the

large-scale channel model on the average received signal power can be tracked well with the state-of-the-art closed-loop power control loops by using control channels such as physical uplink control channel (PUCCH) or physical random access channel (PRACH) in 3GPP Fifth Generation (5G) New Radio (NR) [46]. As a result, the relative positions of the sensors to the UAV do not change our analyses. Note that a similar assumption is also made in [11], [12], [24], where the time-variation in the channel is captured by the realizations of $h_{k,i}$ in (8). In this study, without loss of generality, we set $P_k, \forall k$, to 1 Watt and calculate the signal-to-noise ratio (SNR) of a sensor at the UAV as $\text{SNR} = 1/\sigma_{\text{noise}}^2$.

C. Problem Statement

Suppose that the fading coefficient $h_{k,i}$ is not available at the k th sensor and the UAV due to synchronization impairments, reciprocity calibration errors, or mobility. Under this constraint, the main objective of the UAV is to compute the MV $w_l^{(\ell)}, \forall l$, by exploiting the signal superposition property of the multiple-access channels. Our main goal is to obtain a scheme that computes the MVs with a low probability of incorrect detection without using the fading coefficients at the sensors and the UAV, while the PMEPR of the transmitted signal is guaranteed to be less than a certain value. Although the CSs generated with Theorem 1 can address the latter challenge by keeping the PMEPR of transmitted OFDM signals at most 3 dB, it is not trivial to use them for OAC. In the following section, we show that Theorem 1 can be utilized to construct an OAC scheme to compute MVs without using the CSI at the sensors and the UAV.

III. PROPOSED SCHEME

Given the number of parameters that can be chosen independently in Theorem 1, we consider m MV computations. Let $\mathbf{v}_k^{(\ell)}$ be the vector of m votes of the k th sensor, i.e., $(v_{k,1}^{(\ell)}, \dots, v_{k,m}^{(\ell)})$ for $v_{k,n}^{(\ell)} \in \{-1, 0, 1\}, \forall n$. If $v_{k,n}^{(\ell)} = 0$, i.e., an absentee vote, the k th sensor does not participate in the n th MV computation. Note that the absentee votes have previously been shown to be useful for addressing data heterogeneity for wireless federated learning along with OAC [10]. In particular, to address the scenario discussed in Section II, we set $v_{k,n}^{(\ell)} = \bar{c}_{k,n}^{(\ell)}$ for $n = \{1, 2, 3\}$ and $v_{k,n}^{(\ell)} = 0$ for $n \in \{4, 5, \dots, m\}$ without loss of generality, unless otherwise stated.

The proposed scheme modulates the amplitude of the elements of the CS via $f_r(\mathbf{x})$ as a function of the votes $\mathbf{v}_k^{(\ell)}$ at the k th sensor. To this end, based on Theorem 1, let us denote the functions used at the k th sensor as $f_{r,k}(\mathbf{x})$ and $f_{i,k}(\mathbf{x})$, and their parameters as $\{a_{k,0}^{(\ell)}, a_{k,1}^{(\ell)}, \dots, a_{k,m}^{(\ell)}\}$ and $\{b_{k,0}^{(\ell)}, b_{k,1}^{(\ell)}, \dots, b_{k,m}^{(\ell)}\}$, respectively. To synthesize the transmitted sequence $\mathbf{t}_k^{(\ell)}$ of length $L = 2^m$, we use a fixed permutation π and map $v_{k,n}^{(\ell)}$ to $a_{k,n}^{(\ell)}$ as

$$a_{k,n}^{(\ell)} = \begin{cases} -\xi, & v_{k,n}^{(\ell)} = -1 \\ 0, & v_{k,n}^{(\ell)} = 0 \\ +\xi, & v_{k,n}^{(\ell)} = +1 \end{cases}, \forall n, \quad (9)$$

TABLE II
AN EXAMPLE OF ENCODED CSs BASED ON VOTES FOR $m = 3$.

$\mathbf{v}_k^{(\ell)}$	$t_{k,0}^{(\ell)}$	$t_{k,1}^{(\ell)}$	$t_{k,2}^{(\ell)}$	$t_{k,3}^{(\ell)}$	$t_{k,4}^{(\ell)}$	$t_{k,5}^{(\ell)}$	$t_{k,6}^{(\ell)}$	$t_{k,7}^{(\ell)}$
(0, 0, 0)	1	1	1	-1	1	1	-1	1
(1, 0, 0)	0	$\sqrt{2}$	$\sqrt{2}$	0	0	$\sqrt{2}$	$-\sqrt{2}$	0
(1, 1, 0)	0	0	2	0	0	2	0	0
(1, 1, 1)	0	0	0	0	0	$2\sqrt{2}$	0	0
(1, 1, -1)	0	0	$2\sqrt{2}$	0	0	0	0	0
(1, -1, 0)	0	2	0	0	0	0	-2	0
(-1, 0, 0)	$\sqrt{2}$	0	0	$-\sqrt{2}$	$\sqrt{2}$	0	0	$\sqrt{2}$

where $\xi > 0$ is a scaling parameter. To ensure that the squared ℓ_2 -norm of the CS $\mathbf{t}_k^{(\ell)}$ is 2^m , i.e., $\|\mathbf{t}_k^{(\ell)}\|_2^2 = 2^m$, we choose $a_{k,0}^{(\ell)}$ as

$$a_{k,0}^{(\ell)} = -\frac{1}{2} \sum_{n=1}^m \ln \frac{1 + e^{2a_{k,n}^{(\ell)}}}{2}. \quad (10)$$

To derive (10), notice that $a_{k,n}^{(\ell)}$ scales 2^{m-1} elements of the CS by $e^{a_{k,n}^{(\ell)}}$ in (5) for $n > 0$. Therefore, $\|\mathbf{t}_k^{(\ell)}\|_2^2$ is scaled by $(1 + e^{2a_{k,n}^{(\ell)}})/2$. By considering $a_{k,1}^{(\ell)}, \dots, a_{k,m}^{(\ell)}$, the total scaling can be calculated as $\delta \triangleq \prod_{n=1}^m (1 + e^{2a_{k,n}^{(\ell)}})/2$. Thus, $e^{2a_{k,0}^{(\ell)}} = 1/\delta$ must hold for $\|\mathbf{t}_k^{(\ell)}\|_2^2 = 2^m$, which results in (10).

With (9) and (10), if $v_{k,n}^{(\ell)} \neq 0$ for $\xi \rightarrow \infty$, one half of elements (i.e., the ones for $y_{\pi_n} = 0$) of the CS $\mathbf{t}_k^{(\ell)}$ are set to 0 while the other half (i.e., the ones for $y_{\pi_n} = 1$) are scaled by a factor of $\sqrt{2}$ and the sign of $v_{k,n}^{(\ell)}$ determines which half is amplified. For $v_{k,n}^{(\ell)} = 0$, the halves are not scaled.

Example 1. Let $\boldsymbol{\pi} = (3, 2, 1)$, $H = 2$, $m = 3$, $b_n^{(\ell)} = 0$, $\forall n$. Hence, the indices of the scaled elements are controlled by $y_1 = x_1$, $y_2 = (x_1 + x_2)_2$, and $y_3 = (x_2 + x_3)_2$ when (x_1, x_2, x_3) is listed in lexicographic order, i.e., (0, 0, 0), (0, 0, 1), ..., (1, 1, 1). The encoded CSs for several realizations of $\mathbf{v}_k^{(\ell)}$ for $\xi \rightarrow \infty$ are given in TABLE II. For $\mathbf{v}_k^{(\ell)} = (1, 0, 0)$ and $\mathbf{v}_k^{(\ell)} = (-1, 0, 0)$, four elements determined by y_3 of the uni-modular CS is scaled by $\sqrt{2}$, and the rest is multiplied by 0. Similarly, for $\mathbf{v}_k^{(\ell)} = (1, 1, 1)$ and $\mathbf{v}_k^{(\ell)} = (1, 1, -1)$, four elements of the CS (i.e., the CS for $\mathbf{v}_k^{(\ell)} = (1, 1, 0)$) is scaled by $\sqrt{2}$, and the rest is multiplied with 0. It is worth noting that if all the votes are non-zero, only one of the eight elements of the sequence is non-zero.

For the proposed scheme, the values for $b_{k,0}^{(\ell)}, b_{k,1}^{(\ell)}, \dots, b_{k,m}^{(\ell)}$ are chosen randomly from the set \mathbb{Z}_H for the randomization of $\mathbf{t}_k^{(\ell)}$ across the sensors. This choice is also in line with the cases where phase synchronization cannot be maintained in the network.

Based on (8), the received sequence at the UAV after signal superposition can be expressed as

$$R(z) = \sum_{\forall \mathbf{x} \in \mathbb{Z}_2^m} \underbrace{\left(\sum_{k=1}^K h_{k,i(\mathbf{x})} e^{f_{r,k}(\mathbf{x})} e^{j \frac{2\pi}{H} f_{i,k}(\mathbf{x})} + \omega_i(\mathbf{x}) \right)}_{r_i^{(\ell)}(z)} z^{i(\mathbf{x})}, \quad (11)$$

The scaled halves of the transmitted sequences based on (9) and (10) non-coherently aggregate and the positions of the aggregated elements for the n th MV are determined by y_{π_n} . Thus, to compute the n th MV, the UAV calculates two metrics given by

$$E_n^+ \triangleq \sum_{\substack{\forall \mathbf{x} \in \mathbb{Z}_2^m \\ y_{\pi_n} = 1}} |r_{i(\mathbf{x})}^{(\ell)}|^2 \\ = \sum_{\substack{\forall \mathbf{x} \in \mathbb{Z}_2^m \\ y_{\pi_n} = 1}} \left| \sum_{k=1}^K h_{k,i(\mathbf{x})} e^{f_{r,k}(\mathbf{x})} e^{j \frac{2\pi}{H} f_{i,k}(\mathbf{x})} + \omega_i(\mathbf{x}) \right|^2, \quad (12)$$

and

$$E_n^- \triangleq \sum_{\substack{\forall \mathbf{x} \in \mathbb{Z}_2^m \\ y_{\pi_n} = 0}} |r_{i(\mathbf{x})}^{(\ell)}|^2 \\ = \sum_{\substack{\forall \mathbf{x} \in \mathbb{Z}_2^m \\ y_{\pi_n} = 0}} \left| \sum_{k=1}^K h_{k,i(\mathbf{x})} e^{f_{r,k}(\mathbf{x})} e^{j \frac{2\pi}{H} f_{i,k}(\mathbf{x})} + \omega_i(\mathbf{x}) \right|^2. \quad (13)$$

It then detects the n th MV by comparing the values of E_n^+ and E_n^- as

$$\hat{w}_n^{(\ell)} = \text{sign}(E_n^+ - E_n^-), \forall n. \quad (14)$$

In Fig. 1, we provide the transmitter and receiver block diagrams for the proposed OAC scheme. The k th sensor first estimates the position of the UAV, e.g., by using some image processing [41], [42]. It computes the vector $\mathbf{v}_k^{(\ell)}$ and calculates $\mathbf{t}_k^{(\ell)}$ based on Theorem 1 by using the mapping in (9). It then maps the elements of the encoded CS $\mathbf{t}_k^{(\ell)}$ to 2^m OFDM subcarriers and calculates the N -point inverse discrete Fourier transform (IDFT) of the mapped CS. All the sensors transmit their signals along with a sufficiently large CP duration for OAC. The UAV receives the non-coherently superposed signal. After discarding the CP and calculating the DFT of the remaining received samples, it obtains E_n^+ and E_n^- . The UAV finally detects the MVs with (14) and updates its position based on (1). We discuss the detector performance in (14) rigorously in the following section.

IV. PERFORMANCE ANALYSIS

A. Average Performance

Let K_n^+ , K_n^- , and K_n^0 be the number of sensors with positive, negative, and zero votes for n th MV computation, respectively.

Lemma 1. $\mathbb{E}[E_n^+]$ and $\mathbb{E}[E_n^-]$ can be calculated as

$$\mathbb{E}[E_n^+] = \frac{2^m e^{2\xi} K_n^+}{1 + e^{2\xi}} + \frac{2^m e^{-2\xi} K_n^-}{1 + e^{-2\xi}} + 2^{m-1} (K_n^0 + \sigma_{\text{noise}}^2), \\ \mathbb{E}[E_n^-] = \frac{2^m K_n^+}{1 + e^{2\xi}} + \frac{2^m K_n^-}{1 + e^{-2\xi}} + 2^{m-1} (K_n^0 + \sigma_{\text{noise}}^2),$$

respectively, where the expectation is over the distribution of channel and noise.

The proof is given in Appendix A.

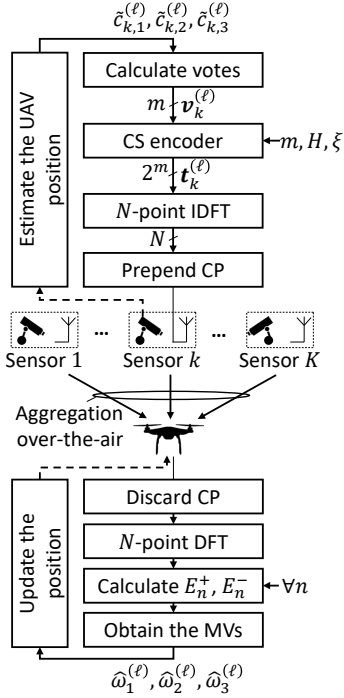


Fig. 1. Transmitter and receiver diagrams for the proposed OAC scheme.

Without any concern about the norm of $\mathbf{t}_k^{(\ell)}$ with (10), we can choose an arbitrarily large ξ , leading to the following result:

Corollary 1. *The following identities hold:*

$$\begin{aligned} \lim_{\xi \rightarrow \infty} \mathbb{E} [E_n^+] &= 2^m K_n^+ + 2^{m-1} K_n^0 + 2^{m-1} \sigma_{\text{noise}}^2, \\ \lim_{\xi \rightarrow \infty} \mathbb{E} [E_n^-] &= 2^m K_n^- + 2^{m-1} K_n^0 + 2^{m-1} \sigma_{\text{noise}}^2. \end{aligned}$$

Based on Corollary 1, we can infer that the detector in (14) is likely to detect the correct MV for $\xi \rightarrow \infty$ since $\lim_{\xi \rightarrow \infty} \mathbb{E} [E_n^+ - E_n^-] = 2^{m-1} (K_n^+ - K_n^-)$ holds. Also, the impact of absentee votes on the metrics E_n^+ and E_n^- are equally shared.

B. Computation Error Rate

For a given set of all votes $\mathbf{V}^{(\ell)} \triangleq (\mathbf{u}_1^{(\ell)}, \dots, \mathbf{u}_m^{(\ell)})$ for $\mathbf{u}_n^{(\ell)} \triangleq (v_{1,n}^{(\ell)}, \dots, v_{K,n}^{(\ell)})$, the CER can be defined as

$$\begin{aligned} \text{CER}(\mathbf{V}^{(\ell)}) &\triangleq \begin{cases} \Pr(E_n^+ - E_n^- < 0; \mathbf{V}^{(\ell)}), & K_n^+ > K_n^- \\ \Pr(E_n^+ - E_n^- > 0; \mathbf{V}^{(\ell)}), & K_n^+ < K_n^- \\ 1, & K_n^+ = K_n^- \end{cases}, \\ &= \begin{cases} F_{E_n^+ - E_n^-}(0; \mathbf{V}^{(\ell)}), & K_n^+ > K_n^- \\ 1 - F_{E_n^+ - E_n^-}(0; \mathbf{V}^{(\ell)}), & K_n^+ < K_n^- \\ 1, & K_n^+ = K_n^- \end{cases}, \end{aligned} \quad (15)$$

where $F_{E_n^+ - E_n^-}(x; \mathbf{V}^{(\ell)})$ is the CDF of $E_n^+ - E_n^-$. It is worth noting that the detector in (14) always makes an error due to

the noisy reception in communication channels when K_n^+ and K_n^- are identical, leading to the third case in (15). For a given $\mathbf{V}^{(\ell)}$, the CDF of $E_n^+ - E_n^-$ can be obtained as follows:

Lemma 2. *Suppose $h_{k,i} \sim \mathcal{CN}(0, 1)$ (i.e., frequency-selective fading) holds. $F_{E_n^+ - E_n^-}(x; \mathbf{V}^{(\ell)})$ can be calculated as*

$$F_{E_n^+ - E_n^-}(x; \mathbf{V}^{(\ell)}) = \frac{1}{2} - \int_{-\infty}^{\infty} \frac{\varphi_n^+(t) \varphi_n^-(t)^*}{2\pi j t} e^{-j t x} dt, \quad (16)$$

respectively, where $\varphi_n^+(t)$ and $\varphi_n^-(t)$ are given by

$$\varphi_n^+(t) \triangleq \prod_{\substack{\forall \mathbf{x} \in \mathbb{Z}_2^m \\ y_{\pi_n} = 1}} \frac{1}{1 - j t \lambda_{i(\mathbf{x})}^{-1}}, \quad (17)$$

and

$$\varphi_n^-(t) \triangleq \prod_{\substack{\forall \mathbf{x} \in \mathbb{Z}_2^m \\ y_{\pi_n} = 0}} \frac{1}{1 - j t \lambda_{i(\mathbf{x})}^{-1}}, \quad (18)$$

respectively, for $\lambda_{i(\mathbf{x})}^{-1} \triangleq \sum_{k=1}^K e^{2f_{r,k}(\mathbf{x})} + \sigma_{\text{noise}}^2$.

The proof is given in Appendix B.

Although $F_{E_n^+ - E_n^-}(x; \mathbf{V}^{(\ell)})$ in (16) is not a closed-form expression, it can be easily evaluated with a numeric integration to compute $\text{CER}(\mathbf{V}^{(\ell)})$ in (15). Also, as demonstrated in Section VI (i.e., Fig. 3), (16) holds approximately in the flat-fading channels since the values for $b_{k,0}^{(\ell)}, b_{k,1}^{(\ell)}, \dots, b_{k,m}^{(\ell)}$ are chosen randomly in our approach.

Let α , β , and γ denote the probabilities given by $\Pr(v_{k,n}^{(\ell)} > 0)$, $\Pr(v_{k,n}^{(\ell)} < 0)$, and $\Pr(v_{k,n}^{(\ell)} = 0)$, respectively, $\forall k \in \{1, \dots, K\}$ and $\forall n \in \{1, \dots, m\}$.

Corollary 2. *For given K_n^+ , K_n^- , K_n^0 , α , β , and γ , the CER for the n th MV is given by*

$$\begin{aligned} \text{CER}(n; K_n^+, K_n^-, K_n^0) &= \begin{cases} \text{CER}^+(n; K_n^+, K_n^-, K_n^0), & K_n^+ > K_n^- \\ \text{CER}^-(n; K_n^+, K_n^-, K_n^0), & K_n^+ < K_n^- \\ 1, & K_n^+ = K_n^- \end{cases}, \end{aligned} \quad (19)$$

where

$$\begin{aligned} \text{CER}^+(n; K_n^+, K_n^-, K_n^0) &\triangleq \frac{1}{2} - \sum_{\forall \mathbf{V}} \alpha^{N^+} \beta^{N^-} \gamma^{N^0} \int_{-\infty}^{\infty} \frac{\varphi_n^+(t) \varphi_n^-(t)^*}{2\pi j t} dt, \end{aligned} \quad (20)$$

$$\begin{aligned} \text{CER}^-(n; K_n^+, K_n^-, K_n^0) &\triangleq \frac{1}{2} + \sum_{\forall \mathbf{V}} \alpha^{N^+} \beta^{N^-} \gamma^{N^0} \int_{-\infty}^{\infty} \frac{\varphi_n^+(t) \varphi_n^-(t)^*}{2\pi j t} dt, \end{aligned} \quad (21)$$

respectively, where N^+ , N^- , and N^0 are the number of elements in $\dot{\mathbf{V}} \triangleq (\mathbf{u}_1^{(\ell)}, \dots, \mathbf{u}_{n-1}^{(\ell)}, \mathbf{u}_{n+1}^{(\ell)}, \dots, \mathbf{u}_m^{(\ell)})$ with 1, -1, and 0, respectively.

Proof. The probability of a realization of $\dot{\mathbf{V}}$ is $\alpha^{N^+} \beta^{N^-} \gamma^{N^0}$. Thus, the expectation of (15) over the distribution of $\dot{\mathbf{V}}$ leads to (20) and (21). \square

The calculations of (20) and (21) can be intractable due to the enumerations of $\hat{\mathbf{V}}$. To address this issue, we average the CER in (15) over a few realizations of $\mathbf{V}^{(\ell)}$ for a given triplet $\{\alpha, \beta, \gamma\}$ to compute (20) and (21) in Section VI.

Finally, let us define CER by setting it as

$$\text{CER} = \Pr(\hat{w}_n^{(\ell)} \neq w_n^{(\ell)}) , \quad (22)$$

for given α , β , and γ . We can calculate CER as follows:

Corollary 3. For given α , β , and γ , CER is given by

$$\begin{aligned} \text{CER} = & \Pr(\hat{w}_n^{(\ell)} = -1, w_n^{(\ell)} = 1) + \Pr(\hat{w}_n^{(\ell)} = 1, w_n^{(\ell)} = -1) \\ & + \Pr(w_n^{(\ell)} = 0) , \end{aligned} \quad (23)$$

where

$$\begin{aligned} \Pr(\hat{w}_n^{(\ell)} = -1, w_n^{(\ell)} = 1) &= \sum_{l=0}^K \sum_{k=l+1}^{K-l} \binom{K}{k} \binom{K-k}{l} \alpha^k \beta^l \gamma^{K-k-l} \text{CER}^+(n; k, l, m) , \\ \Pr(\hat{w}_n^{(\ell)} = 1, w_n^{(\ell)} = -1) &= \sum_{k=0}^K \sum_{l=k+1}^{K-k} \binom{K}{k} \binom{K-k}{l} \alpha^k \beta^l \gamma^{K-k-l} \text{CER}^-(n; k, l, m) , \\ \Pr(w_n^{(\ell)} = 0) &= \sum_{k=0}^{\lfloor \frac{K}{2} \rfloor} \binom{K}{k} \binom{K-k}{k} \alpha^k \beta^k \gamma^{K-2k} . \end{aligned}$$

The third term in (23) is because of the third case in (19). In Section VI, we evaluate CER for different α , β , and γ values.

C. Computation Rate and Resource Utilization Ratio

The computation rate \mathcal{R} can be defined as the number of functions computed per channel use (in real dimension) [8], [47]. Since the proposed scheme computes m MVs over 2^m complex-valued resources, \mathcal{R} can be expressed as

$$\mathcal{R} = \frac{m}{2^{m+1}} . \quad (24)$$

Hence, for a larger m , the computation rate reduces while the CER improves significantly as demonstrated in Section VI.

Let us define the resource utilization ratio as the ratio between the number of resources consumed with the proposed scheme and the number of resources when the communication and computation are considered as separate tasks, i.e., the traditional first-communicate-then-compute approach. For the separation, we assume that the spectral efficiency is r bit/s/Hz. Hence, the resources needed for K EDs and m bits (i.e., votes) can be obtained as mK/r . The proposed scheme consumes 2^m complex-valued resources for K EDs. Hence, the resource utilization ratio can be expressed as

$$\epsilon = \frac{2^m}{mK/r} . \quad (25)$$

For instance, for $r = 1$ bit/s/Hz, $m = 7$, and $K = 50$, the wireless resources needed with the proposed scheme is $\epsilon = 0.3657$ times the ones with the traditional approach.

D. Complexity Analysis

As can be seen from Theorem 1, the functions $f_{r,k}(\mathbf{x})$ and $f_{i,k}(\mathbf{x})$ alter the coefficients of the first-order monomials. Hence, *without* a recursive method, $m2^m$ real-valued sum operations must be performed to calculate the functions $f_{r,k}(\mathbf{x})$ and $f_{i,k}(\mathbf{x})$, and the multiplication operations can be replaced with multiplexers as \mathbf{x} has binary elements. Also, 2^m multiplications are required to compute the elements of $\mathbf{t}_k^{(\ell)}$. Thus, the computation complexity at the transmitter is $\mathcal{O}(2^m)$. However, if the recursive construction of the RM codes is exploited, the number of operations asymptotically scales with $\log_2(2^m)$, resulting in a computation complexity of $\mathcal{O}(m)$. At the receiver, (12) and (13) are calculated to obtain m MVs, which require at least 2^m complex multiplications to compute the magnitude squares of the elements of the received sequence. Hence, the computation complexity at the receiver is $\mathcal{O}(2^m)$, i.e., a linearly increased complexity with the length of CS.

V. CONVERGENCE ANALYSIS

In this section, we discuss the convergence of the resulting systems under the control strategies in (3) by analyzing their Lyapunov stability based on the following definition:

Definition 1 ([48]). A stochastic system $x^{(\ell+1)} = f(x^{(\ell)})$, where f describes the dynamics and $x^{(\ell)}$ is the state, is called globally uniformly ultimately bounded in mean square with ultimate bound b , if there exist positive b and L such that for any $\mathbb{E}[\|x^{(0)}\|^2] < \infty$, the inequality $\mathbb{E}[\|x^{(\ell)}\|^2] \leq b$ holds for all $\ell \geq L$.

We define $\delta_l^{(\ell)}$ by setting $\delta_l^{(\ell)} = c_l^{(\ell)} - c_{t,l}$ and re-express (1) as

$$\delta_l^{(\ell+1)} = \delta_l^{(\ell)} - T_{\text{update}} u_l^{(\ell)} . \quad (26)$$

for the convergence analysis of each case in (3).

A. Case 1: Continuous Update & Ideal Communications

The control strategy can be written as

$$g_l^{(\ell)} = \frac{1}{K} \sum_{k=1}^K \left(c_l^{(\ell)} + \epsilon_{k,l}^{(\ell)} - c_{t,l} \right) = \delta_l^{(\ell)} + \frac{1}{K} \sum_{k=1}^K \epsilon_{k,l}^{(\ell)} .$$

Since $\epsilon_{k,l}^{(\ell)}$ is Gaussian and the summands are independent of each other, $\frac{1}{K} \sum_{k=1}^K \epsilon_{k,l}^{(\ell)}$ is also Gaussian. Based on stochastic control theory [49], as long as $|1 - \mu T_{\text{update}}| < 1$, the resulting closed-loop system is stable in a stochastic sense.

B. Case 2: MV-based Update & Ideal Communications

In this case, $|g_l^{(\ell)}|$ is at most 1. Therefore, as long as $\mu \leq u_{\text{limit}}$, input saturation will not happen and the dynamic can be written as

$$\begin{aligned} \delta_l^{(\ell+1)} &= \delta_l^{(\ell)} - \mu T_{\text{update}} \text{sign} \left(\sum_{k=1}^K \bar{c}_{k,l}^{(\ell)} \right) \\ &= \delta_l^{(\ell)} - \mu T_{\text{update}} g_l^{(\ell)} . \end{aligned} \quad (27)$$

Recall that $\bar{c}_{k,l}^{(\ell)} = \text{sign}(\bar{c}_{k,l}^{(\ell)} - c_{t,l}) = \text{sign}(\delta_l^{(\ell)} + \epsilon_{k,l}^{(\ell)})$ and $\epsilon_{k,l}^{(\ell)}$ is Gaussian. We can then obtain the values of α , β , and γ as

$$\begin{aligned} \alpha &= \Pr(\bar{c}_{k,l}^{(\ell)} = +1) = \Pr(\delta_l^{(\ell)} + \epsilon_{k,l}^{(\ell)} > 0) \\ &= \Pr\left(\frac{\epsilon_{k,l}^{(\ell)}}{\sigma_s} > \frac{-\delta_l^{(\ell)}}{\sigma_s}\right) = 1 - \Phi\left(\frac{-\delta_l^{(\ell)}}{\sigma_s}\right), \end{aligned} \quad (28)$$

$$\begin{aligned} \beta &= \Pr(\bar{c}_{k,l}^{(\ell)} = -1) = \Pr(\delta_l^{(\ell)} + \epsilon_{k,l}^{(\ell)} < 0) \\ &= \Pr\left(\frac{\epsilon_{k,l}^{(\ell)}}{\sigma_s} < \frac{-\delta_l^{(\ell)}}{\sigma_s}\right) = \Phi\left(\frac{-\delta_l^{(\ell)}}{\sigma_s}\right), \end{aligned} \quad (29)$$

$$\gamma = \Pr(\bar{c}_{k,l}^{(\ell)} = 0) = 0,$$

respectively. With the distribution of $\bar{c}_{k,l}^{(\ell)}$, we have

$$\phi_+(\delta_l^{(\ell)}) \triangleq \Pr(g_l^{(\ell)} = +1) = \sum_{k=0}^{\lceil \frac{K}{2} \rceil - 1} \binom{K}{k} \alpha^{K-k} \beta^k, \quad (30)$$

$$\phi_-(\delta_l^{(\ell)}) \triangleq \Pr(g_l^{(\ell)} = -1) = \sum_{k=0}^{\lceil \frac{K}{2} \rceil - 1} \binom{K}{k} \alpha^k \beta^{K-k}, \quad (31)$$

$$\phi_0(\delta_l^{(\ell)}) \triangleq \begin{cases} 0, & \text{odd } K \\ \binom{K}{K/2} \alpha^{\frac{K}{2}} \beta^{\frac{K}{2}}, & \text{even } K \end{cases}. \quad (32)$$

Given the distribution of $g_l^{(\ell)}$, we can show the convergence of the system under the MV (ideal) case:

Theorem 2. *Given $\mu \leq u_{\text{limit}}$, the system in (26) is globally uniformly ultimately bounded in mean square under the MV (ideal) control strategy in (3).*

Proof. Let $V(x) \triangleq x^2$. Then, by using (27),

$$\begin{aligned} \mathbb{E} \left[V(\delta_l^{(\ell+1)}) | \delta_l^{(\ell)} \right] - V(\delta_l^{(\ell)}) & \quad (33) \\ &= -2\mu T_{\text{update}} \mathbb{E} \left[g_l^{(\ell)} | \delta_l^{(\ell)} \right] \delta_l^{(\ell)} + \mu^2 T_{\text{update}}^2 \mathbb{E} \left[(g_l^{(\ell)})^2 | \delta_l^{(\ell)} \right]. \end{aligned}$$

By using (30) and (31),

$$\mathbb{E} \left[g_l^{(\ell)} | \delta_l^{(\ell)} \right] = \phi_+(\delta_l^{(\ell)}) - \phi_-(\delta_l^{(\ell)}), \quad (34)$$

$$\mathbb{E} \left[(g_l^{(\ell)})^2 | \delta_l^{(\ell)} \right] = \phi_+(\delta_l^{(\ell)}) + \phi_-(\delta_l^{(\ell)}) \in [0, 1]. \quad (35)$$

Therefore, by using (34) and (35), (33) yields

$$\begin{aligned} & \mathbb{E} \left[V(\delta_l^{(\ell+1)}) | \delta_l^{(\ell)} \right] - V(\delta_l^{(\ell)}) \\ &= -2\mu T_{\text{update}} \left(\phi_+(\delta_l^{(\ell)}) - \phi_-(\delta_l^{(\ell)}) \right) \delta_l^{(\ell)} \\ & \quad + \mu^2 T_{\text{update}}^2 \left(\phi_+(\delta_l^{(\ell)}) + \phi_-(\delta_l^{(\ell)}) \right) \\ & \leq -2\mu T_{\text{update}} \left(\phi_+(\delta_l^{(\ell)}) - \phi_-(\delta_l^{(\ell)}) \right) \delta_l^{(\ell)} + \mu^2 T_{\text{update}}^2. \end{aligned}$$

Note that $\delta_l^{(\ell)} > 0 \Rightarrow \phi_+(\delta_l^{(\ell)}) > \phi_-(\delta_l^{(\ell)})$ and $\delta_l^{(\ell)} < 0 \Rightarrow \phi_+(\delta_l^{(\ell)}) < \phi_-(\delta_l^{(\ell)})$, which means

$$\left(\phi_+(\delta_l^{(\ell)}) - \phi_-(\delta_l^{(\ell)}) \right) \delta_l^{(\ell)} > 0,$$

always holds. Meanwhile, $\left(\phi_+(\delta_l^{(\ell)}) - \phi_-(\delta_l^{(\ell)}) \right) \delta_l^{(\ell)}$ is monotonic increasing when $\delta_l^{(\ell)} > 0$ and monotonic decreasing when $\delta_l^{(\ell)} < 0$ with the global minimum at $\delta_l^{(\ell)} = 0$. Thus, we can define

$$\gamma = \max_{q \in \mathbb{R}} |q|, \quad \text{s.t.} \quad \left(\phi_+(q) - \phi_-(q) \right) q = \frac{\mu T_{\text{update}}}{2},$$

and the parameter γ must be finite, whose value depends on μT_{update} and σ_s . For any $\delta_l^{(\ell)}$ such that $|\delta_l^{(\ell)}| > \gamma$, we have

$$\left(\phi_+(\delta_l^{(\ell)}) - \phi_-(\delta_l^{(\ell)}) \right) \delta_l^{(\ell)} > \frac{\mu T_{\text{update}}}{2},$$

and then

$$\mathbb{E} \left[V(\delta_l^{(\ell+1)}) | \delta_l^{(\ell)} \right] - V(\delta_l^{(\ell)}) < 0.$$

Thus, the system is mean-square globally uniformly ultimately bounded and the mean-square ultimate bound is determined by γ . \square

C. Case 3: MV with the Proposed OAC

By using Corollary 2, we can re-calculate $\phi_+(\delta_l^{(\ell)})$ and $\phi_-(\delta_l^{(\ell)})$ defined in (30) and (31), respectively, as

$$\phi_+(\delta_l^{(\ell)}) = 1 - \underbrace{\sum_{k=0}^K \binom{K}{k} \alpha^k \beta^{K-k} \text{CER}^+(n; k, K-k, 0)}_{\triangleq \zeta},$$

$$\phi_-(\delta_l^{(\ell)}) = 1 - \phi_+(\delta_l^{(\ell)}),$$

where α and β are given in (28) and (29), respectively. Now the convergence of the system under the OAC (MV) strategy is presented in the following theorem:

Theorem 3. *Given $\mu \leq u_{\text{limit}}$, the system in (26) is globally uniformly ultimately bounded in mean square under the MV (OAC) control strategy in (14).*

Proof. Similar to the proof of Theorem 2, let $V(x) \triangleq x^2$ and we have

$$\begin{aligned} \mathbb{E} \left[V(\delta_l^{(\ell+1)}) | \delta_l^{(\ell)} \right] - V(\delta_l^{(\ell)}) & \\ &= -2\mu T_{\text{update}} \mathbb{E} \left[g_l^{(\ell)} | \delta_l^{(\ell)} \right] \delta_l^{(\ell)} + \mu^2 T_{\text{update}}^2 \mathbb{E} \left[(g_l^{(\ell)})^2 | \delta_l^{(\ell)} \right]. \end{aligned}$$

Based on the distribution of $g_l^{(\ell)}$ for the OAC (MV) case,

$$\mathbb{E} \left[g_l^{(\ell)} | \delta_l^{(\ell)} \right] = \phi_+(\delta_l^{(\ell)}) - \phi_-(\delta_l^{(\ell)}) = 1 - 2\zeta,$$

$$\mathbb{E} \left[(g_l^{(\ell)})^2 | \delta_l^{(\ell)} \right] = 1.$$

Therefore,

$$\begin{aligned} & \mathbb{E} \left[V(\delta_l^{(\ell+1)}) | \delta_l^{(\ell)} \right] - V(\delta_l^{(\ell)}) \\ &= -2\mu T_{\text{update}} \left(\phi_+(\delta_l^{(\ell)}) - \phi_-(\delta_l^{(\ell)}) \right) \delta_l^{(\ell)} + \mu^2 T_{\text{update}}^2. \end{aligned}$$

Note that $\zeta < 1/2$ for $\delta_l^{(\ell)} > 0$ and $\zeta > 1/2$ for $\delta_l^{(\ell)} < 0$ with the proposed OAC scheme, which means

$$\left(\phi_+(\delta_l^{(\ell)}) - \phi_-(\delta_l^{(\ell)}) \right) \delta_l^{(\ell)} > 0,$$

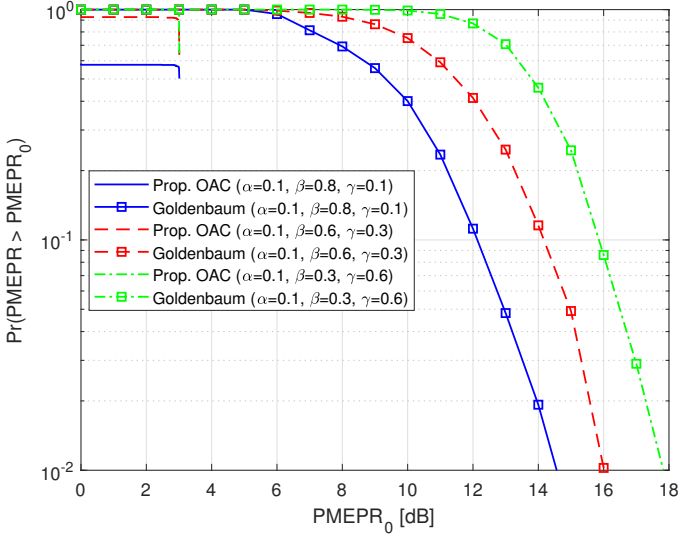


Fig. 2. PMEPR distribution.

always holds. Thus, following a similar analysis in the proof of Theorem 2, we conclude that the system is mean-square globally uniformly ultimately bounded and the ultimate bound is determined by μT_{update} and σ_s . \square

VI. NUMERICAL RESULTS

In this section, we first numerically analyze the performance of the scheme for an arbitrary application. Subsequently, we apply it to the UAV waypoint flight control scenario discussed in Section II. For all analyses, we assume that there are $K = 50$ sensors. For comparison, we also generate our results with Goldenbaum's non-coherent OAC scheme discussed in [31]. In this approach, the power of the transmitted signal is modulated. To this end, a transmitter maps three possible votes, i.e., -1 , 0 , and 1 , to the symbols 0 , 1 , and 2 , respectively, and multiplies a unimodular random sequence of length L with the square of the symbol to be aggregated. The receiver calculates the norm-square of the aggregated sequences and re-scales it with $f(x) = x/L - K$. It then calculates the sign of scaled value to obtain the MV. To make a fair comparison, L is set to the nearest integer to $2^m/m$, and m sequences are mapped to the subcarriers back-to-back to compute m MVs. For instance, for $m = 6$, our scheme computes 6 MVs by using 64 resources, i.e., 64 OFDM subcarriers. Hence, we choose L to be 11 as $2^m/m \approx 10.67$ and use orthogonal resources to compute 6 MVs for Goldenbaum's approach. We choose the phase of an element of unimodular sequence uniformly between 0 and 2π . Note that the relative positions of the sensors to the UAV and the room shape do not alter the performance of the evaluated schemes due to the power control assumption and sensor model discussed in Section II.

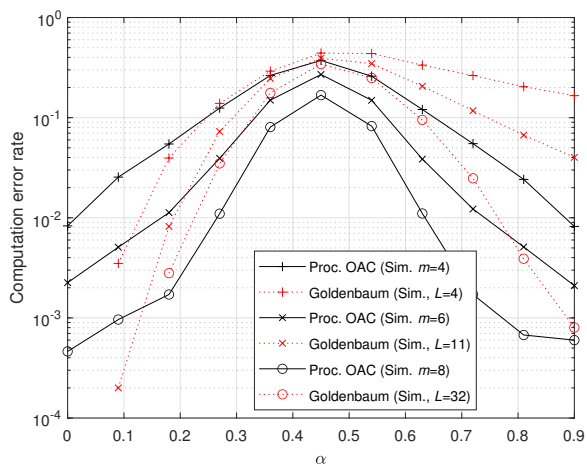
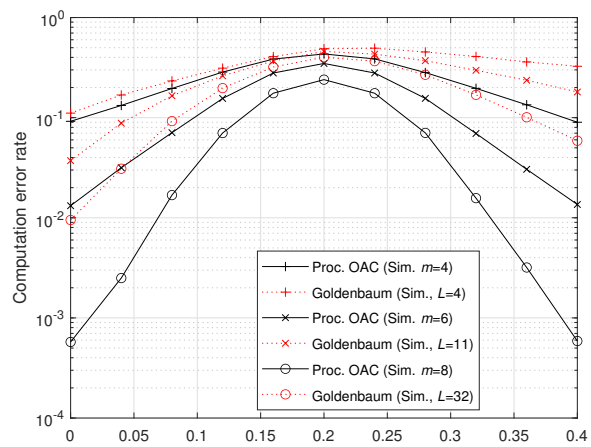
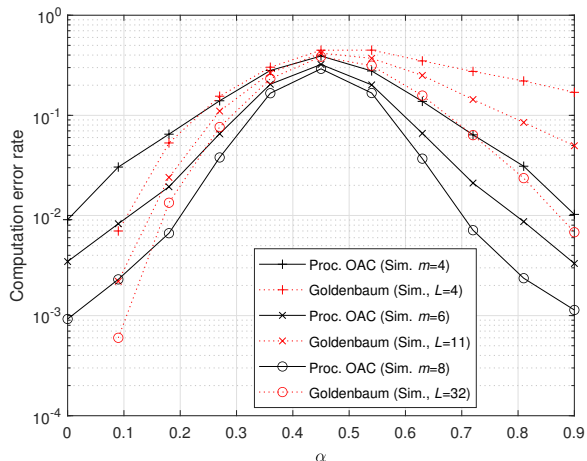
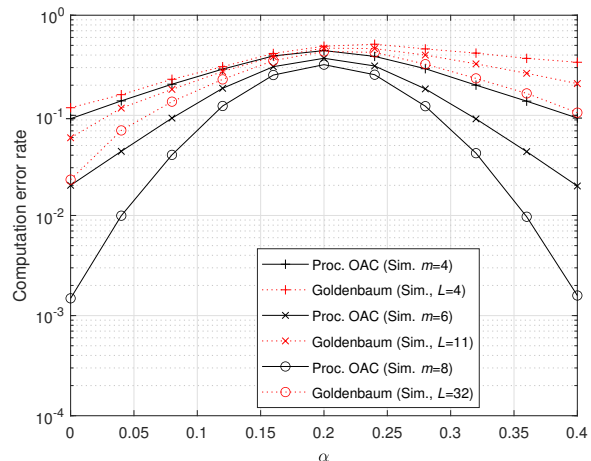
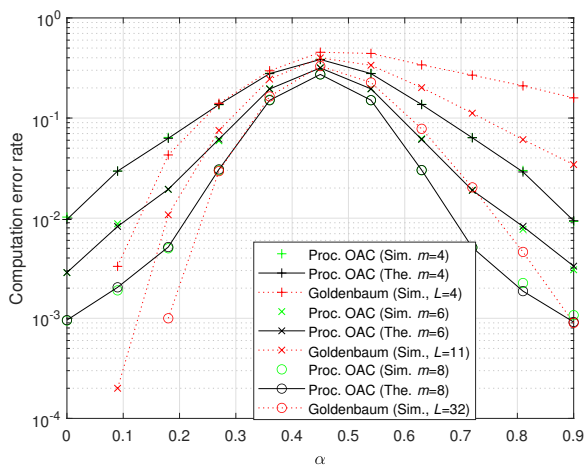
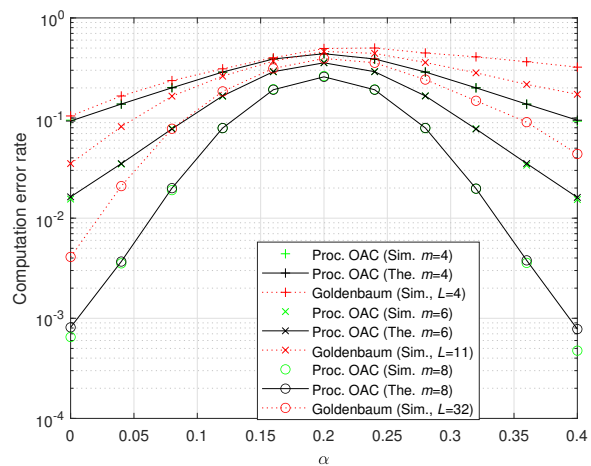
A. CER and PMEPR Results

In Fig. 2, we analyze the PMEPR distribution of the transmitted signals for $m = 8$, $L = 32$, $\alpha = 0.1$, and $\gamma \in \{0.1, 0.3, 0.6\}$. As can be seen from Fig. 2, the PMEPR

of a transmitted signal with the proposed scheme is always less than or equal to 3 dB due to the properties of the CSs. If there are no absentee votes, the maximum PMEPR of the proposed scheme is 0 dB since a single subcarrier is used for the transmission (see the cases for $\mathbf{v}_k^{(\ell)} = (1, 1, 1)$ and $\mathbf{v}_k^{(\ell)} = (1, 1, -1)$ in Example 1). Hence, for a larger absentee vote probability, the probability of observing 0 dB PMEPR increases. The combination of sequences that lead to 0 dB and 3 dB PMEPR values and results in the jumps in the PMEPR distribution given in Fig. 2. The PMEPR characteristics for Goldenbaum's approach are similar to the ones for typical OFDM transmissions and the gap between the proposed scheme and Goldenbaum's approach is considerable large in term of PMEPR.

In Fig. 3, we analyze CER defined in (22) for $\gamma \in \{0.1, 0.6\}$, $m = \{4, 6, 8\}$ for the proposed scheme and $L = \{4, 11, 32\}$ for Goldenbaum's approach by sweeping α in flat-fading (i.e., $h_{k,i} = h_{k,i'} \sim \mathcal{CN}(0, 1)$, $i \neq i'$ for Rayleigh distribution and $h_{k,i} = h_{k,i'} = e^{j2\pi\theta_{k,i}}$, $\theta_{k,i} \sim \mathcal{U}_{[0,1]}$, $i \neq i'$ for Rice distribution with an infinite Rician K -factor) and frequency-selective (i.e., $h_{k,i} \sim \mathcal{CN}(0, 1)$) channels, respectively. For both schemes, as expected, the CER improves for a small or a large α since more sensors vote for -1 or $+1$, respectively. The performance in the frequency selective channel is slightly better than the ones in flat-fading channels because of the diversity gain. Also, both schemes achieve a better CER for increasing m or L at the expense of more resource consumption in all channel conditions. When α and γ are small (as in Fig. 3(a), Fig. 3(c) and Fig. 3(e)), most of the votes are -1 . In this case, the norm square of the superposed sequence, calculated at the receiver for Goldenbaum's scheme, becomes less sensitive to the fading coefficients as most of the sensors are silent. On the contrary, if α gets larger, the norm square of the superposed sequence fluctuates based on the fading coefficients. As a result, the corresponding detector performs poorly compared to the case with smaller α . Thus, Goldenbaum's scheme exhibits an unbalanced behavior across different α values. In contrast, the proposed scheme does not show such unbalanced characteristics while improving the performance in most cases. For $\gamma = 0.1$, the proposed scheme performs better than Goldenbaum's approach for $\alpha \in [0.27, 0.8]$. When there are more absentee votes, i.e., $\gamma = 0.6$, the proposed scheme is superior to Goldenbaum's scheme for all values of α , as can be seen in Fig. 3(b), Fig. 3(d) and Fig. 3(f). Also, the theoretical CERs based on the expression in (23) are well-aligned with the simulation results in Fig. 3(e) and Fig. 3(f).

In Fig. 4, we evaluate $\text{CER}(n; K_n^+, K_n^-, K_n^0)$ in Corollary 2 in frequency-selective fading channel by increasing K_n^+ from 22 to 40 for $K_n^0 = 10$ (i.e., the first case of (19)), SNR = 10 dB, $m \in \{3, 4, 5, 6, 7\}$ for the proposed scheme and $L \in \{3, 4, 6, 11, 18\}$ for the Goldenbaum's approach. In Fig. 4(a), we assume $\alpha = 1$, $\beta = 0$, and $\gamma = 0$ (or $\alpha = 0$, $\beta = 1$, and $\gamma = 0$). As $\gamma = 0$, there are no absentee votes. Also, the same number of sensors activates the same element of the transmitted sequence for all realizations. Since the other elements are not used for the transmission and the energy

(a) Flat fading (Rice distribution, infinite K -factor, $\gamma = 0.1$).(b) Flat fading (Rice distribution, infinite K -factor, $\gamma = 0.6$).(c) Flat fading (Rayleigh distribution, $\gamma = 0.1$).(d) Flat fading (Rayleigh distribution, $\gamma = 0.6$).(e) Frequency-selective fading (Rayleigh distribution, $\gamma = 0.1$).(f) Frequency-selective fading (Rayleigh distribution, $\gamma = 0.6$).Fig. 3. CER for flat and frequency-selective channels ($K = 50$ sensors).

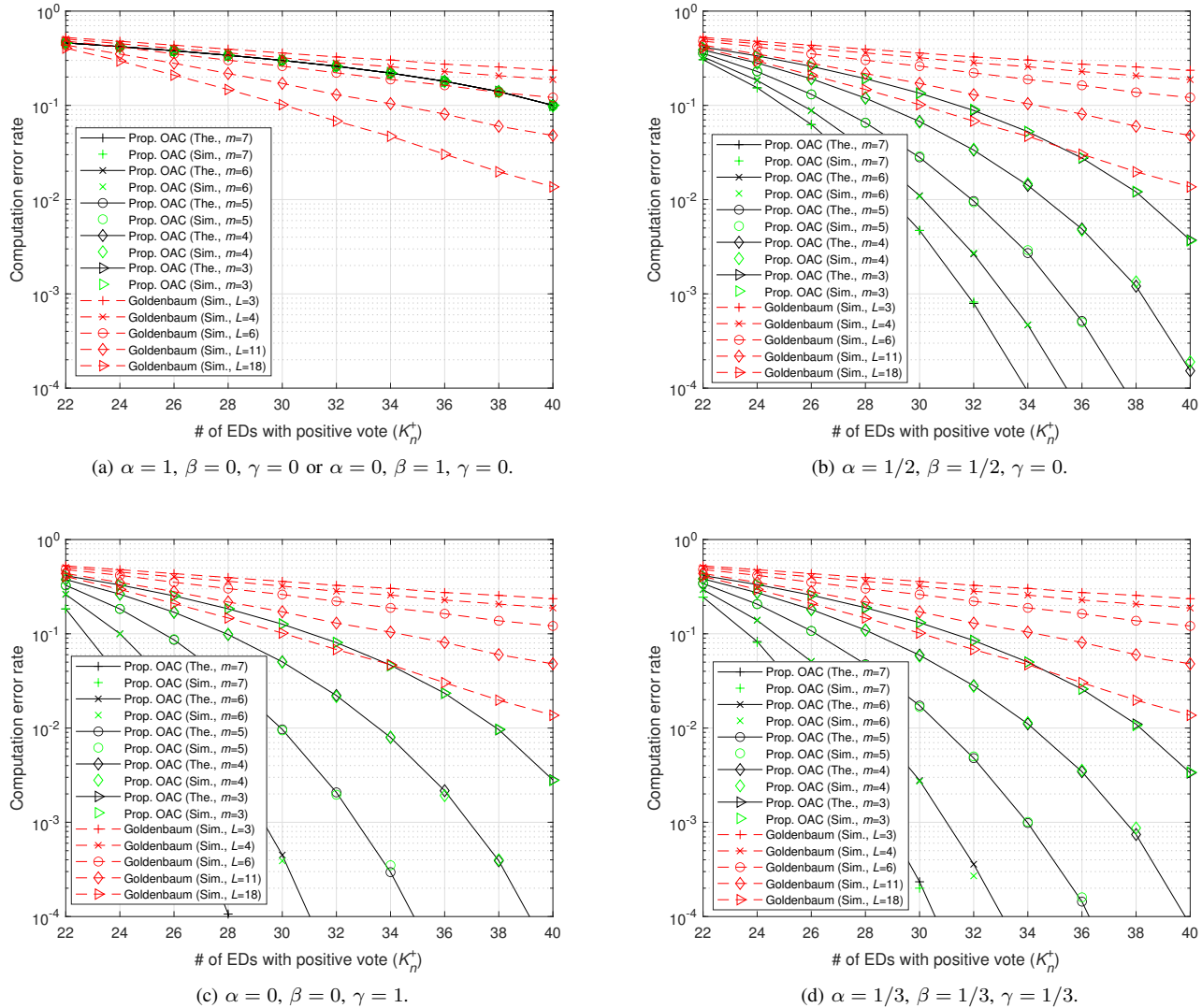


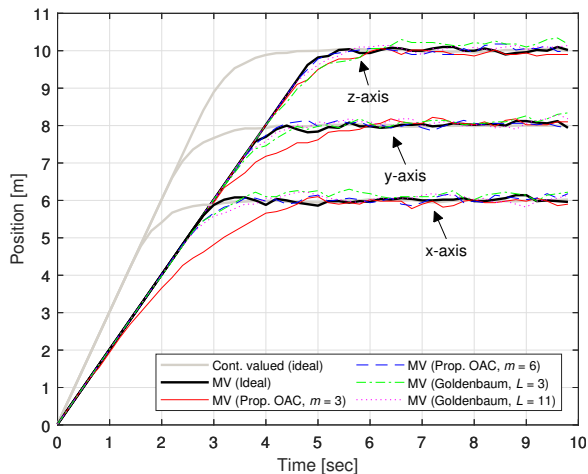
Fig. 4. $\text{CER}^+(n; K_n^+, K_n^-, K_n^0)$ for different values of α, β, γ ($K = 50$ EDs, $K_n^0 = 10$ EDs, SNR = 10 dB, frequency-selective fading channel).

accumulation is non-coherent, the scheme does not provide any performance gain with increasing m . In Fig. 4(b), we assume that $\alpha = 1/2, \beta = 1/2$, and $\gamma = 0$. As compared to the previous case, we observe a significant improvement with increasing m . This is because the randomness enables the votes to accumulate on 2^{m-1} subcarriers, rather than a single resource. Hence, accumulating the energy over multiple subcarriers yields a better estimation of E_n^+ and E_n^- . A similar result is given in Fig. 4(c) when all the sensors have absentee votes, i.e., $\alpha = 0, \beta = 0$, and $\gamma = 1$. This is due to the fact that all sensors activate 2^{m-1} elements of the transmitted CS. Hence, the CER decreases when m increases. Finally, in Fig. 4(d), we analyze the case for $\alpha = 1/3, \beta = 1/3$, and $\gamma = 1/3$ and show that CER performance improves with increasing m . For all cases, the theoretical results match with the simulations, and the CER performance improves with increasing K_n^+ . For Goldenbaum's scheme, each MV is calculated on orthogonal resources. Hence, the corresponding $\text{CER}(n; K_n^+, K_n^-, K_n^0)$ is not a function of α, β , and γ . We

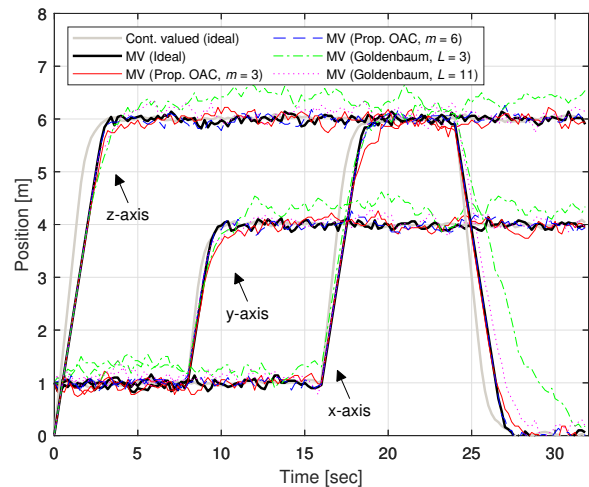
observe that Goldenbaum's scheme performs better for a larger L . However, since the proposed scheme can exploit the available number of subcarriers much more effectively, it yields notably better performance, as seen in Fig. 4(b)-(d).

B. UAV Waypoint Flight Control

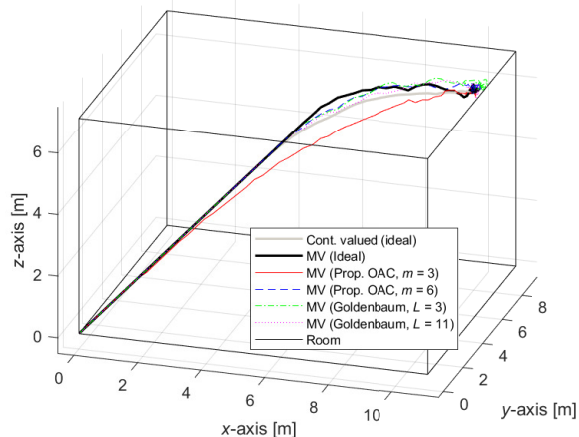
In Fig. 5 and Fig. 6, we consider the UAV waypoint flight control scenario discussed in Section II for $K = 50$ sensors. We assume $T_{\text{update}} = 10$ ms, $\mu = 2$, $u_{\text{limit}} = 3$ m/s, $\sigma_s^2 = 2$, and SNR = 10 dB. We provide the trajectory of the UAV in time and space. We consider two cases. In the first case, there is only one point of interest $(c_{t,1}, c_{t,2}, c_{t,3}) = (10, 8, 6)$ and the initial position of the UAV is $(0, 0, 0)$. In the second case, the points of interest are $(1, 1, 6), (1, 4, 6), (6, 4, 6)$, and $(6, 4, 0)$, where the initial position of the UAV is $(1, 1, 0)$. We compare the proposed scheme for $m \in \{3, 6\}$ with both continuous and MV-based feedback in an ideal communication channel (i.e., no error due to the communication) and Goldenbaum's approach for $L \in \{3, 11\}$. As can be seen



(a) UAV's trajectory in time.



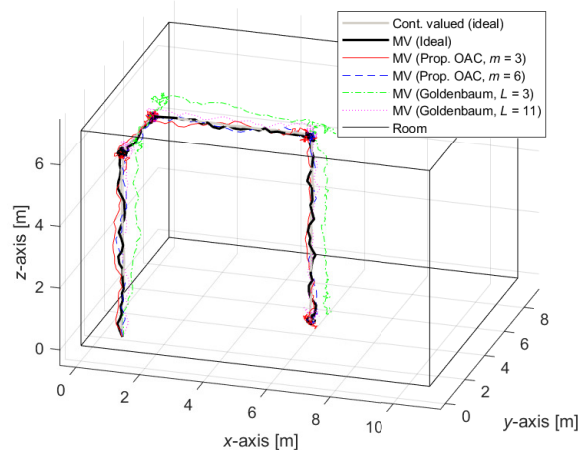
(a) UAV's trajectory in time.



(b) UAV's trajectory in space.

Fig. 5. UAV's trajectory with a single point of interest. The initial position is $(0, 0, 0)$ and the target position is $(10, 8, 6)$.

from Fig. 5(a), for the continuous-valued feedback, the UAV reaches its position faster than any MV-based approach. This is because the velocity increment is limited by the step size for MV-based feedback in our setup. Hence, as can be seen from Fig. 5(b), the UAV's trajectory in space is slightly bent. Since the proposed scheme is also based on the MV computation, its characteristics are similar to the one with MV computation in an ideal channel. Since the CER with $m = 6$ is lower than the one with $m = 3$, the proposed scheme for $m = 6$ performs better and its characteristics are similar to the ideal MV-based feedback. Goldenbaum's approach has similar characteristics to the proposed scheme in terms of trajectory. However, the variation of the UAV position is considerably large when the UAV reaches its final point, as can be seen in Fig. 5(b), in particular for $L = 3$. The position of the UAV in time and space for multiple points of interest is given in Fig. 6(a) and Fig. 6(b), respectively. The proposed scheme for $m = 6$ performs similarly to the one with the MVs in ideal communications, and increasing m leads to a more stable trajectory. For $L = 3$, the trajectory is less stable for



(b) UAV's trajectory in space.

Fig. 6. UAV's trajectory with multiple points of interest, i.e., $(1, 1, 6)$, $(1, 4, 6)$, $(6, 4, 6)$, and $(6, 4, 0)$. The initial position is $(1, 1, 0)$.

Goldenbaum's method. However, its performance improves for a larger L for Goldenbaum's approach.

VII. CONCLUDING REMARKS

In this study, we modulate the amplitude of the CS based on Theorem 1 to develop a new non-coherent OAC scheme for MV computation. We show that the proposed scheme reduces the CER via bandwidth expansion in flat-fading and frequency-selective fading channel conditions while maintaining the PMEPR of the transmitted OFDM signals to be less than or equal to 3 dB. In this work, we derive the theoretical CER and provide the convergence analyses for a control scenario. We show that the proposed scheme results in a lower CER than Goldenbaum's method while providing a significant PMEPR gain. Finally, we demonstrate its applicability to a flight control scenario. The proposed scheme with a larger length of sequences performs similarly to the case where MV without OAC. The proposed approach can also be utilized in other applications, such as wireless federated learning or distributed optimization over wireless networks using MV

computation, to address the congestion problems in band-limited wireless channels.

APPENDIX A
PROOF OF LEMMA 1

We first need the following proposition:

Proposition 1. *The following identities hold:*

$$\sum_{\substack{\forall \mathbf{x} \in \mathbb{Z}_2^m \\ y_{\pi_n}=1}} e^{2f_{r,k}(\mathbf{x})} = e^{2a_{k,n}^{(\ell)}} \sum_{\substack{\forall \mathbf{x} \in \mathbb{Z}_2^m \\ y_{\pi_n}=0}} e^{2f_{r,k}(\mathbf{x})} = \frac{e^{2a_{k,n}^{(\ell)}} 2^m}{1 + e^{2a_{k,n}^{(\ell)}}}.$$

Proof. The first identity is because $e^{2a_{k,n}^{(\ell)} y_{\pi_n}} = 1$ for $y_{\pi_n} = 0$. Under (10), $\|\mathbf{t}_k^{(\ell)}\|_2^2 = 2^m$ holds. Hence,

$$\begin{aligned} \|\mathbf{t}_k^{(\ell)}\|_2^2 &= \sum_{\forall \mathbf{x} \in \mathbb{Z}_2^m} e^{2f_{r,k}(\mathbf{x})} = \sum_{\substack{\forall \mathbf{x} \in \mathbb{Z}_2^m \\ y_{\pi_n}=0}} e^{2f_{r,k}(\mathbf{x})} + \sum_{\substack{\forall \mathbf{x} \in \mathbb{Z}_2^m \\ y_{\pi_n}=1}} e^{2f_{r,k}(\mathbf{x})} \\ &= \sum_{\substack{\forall \mathbf{x} \in \mathbb{Z}_2^m \\ y_{\pi_n}=0}} e^{2f_{r,k}(\mathbf{x})} + e^{2a_{k,n}^{(\ell)}} \sum_{\substack{\forall \mathbf{x} \in \mathbb{Z}_2^m \\ y_{\pi_n}=0}} e^{2f_{r,k}(\mathbf{x})} = 2^m. \end{aligned}$$

□

Proof of Lemma 1. By using Proposition 1, we can calculate $\mathbb{E}[E_n^+]$ and $\mathbb{E}[E_n^-]$ as

$$\begin{aligned} \mathbb{E}[E_n^+] &= \sum_{\substack{\forall \mathbf{x} \in \mathbb{Z}_2^m \\ y_{\pi_n}=1}} \mathbb{E} \left[\left| \sum_{k=1}^K h_{k,i}(\mathbf{x}) e^{f_{r,k}(\mathbf{x})} e^{j \frac{2\pi}{H} f_{i,k}(\mathbf{x})} + \omega_i(\mathbf{x}) \right|^2 \right] \\ &= \sum_{k=1}^K \sum_{\substack{\forall \mathbf{x} \in \mathbb{Z}_2^m \\ y_{\pi_n}=1}} e^{2f_{r,k}(\mathbf{x})} + 2^{m-1} \sigma_{\text{noise}}^2 \\ &= \sum_{k=1}^K \frac{e^{2a_{k,n}^{(\ell)}} 2^m}{1 + e^{2a_{k,n}^{(\ell)}}} + 2^{m-1} \sigma_{\text{noise}}^2 \\ &= 2^m \left(\frac{e^{2\xi}}{1 + e^{2\xi}} K_n^+ + \frac{1}{2} K_n^0 + \frac{e^{-2\xi}}{1 + e^{-2\xi}} K_n^- + \frac{1}{2} \sigma_{\text{noise}}^2 \right), \end{aligned}$$

and

$$\begin{aligned} \mathbb{E}[E_n^-] &= \sum_{\substack{\forall \mathbf{x} \in \mathbb{Z}_2^m \\ y_{\pi_n}=0}} \mathbb{E} \left[\left| \sum_{k=1}^K h_{k,i}(\mathbf{x}) e^{f_{r,k}(\mathbf{x})} e^{j \frac{2\pi}{H} f_{i,k}(\mathbf{x})} + \omega_i(\mathbf{x}) \right|^2 \right] \\ &= \sum_{k=1}^K \sum_{\substack{\forall \mathbf{x} \in \mathbb{Z}_2^m \\ y_{\pi_n}=0}} e^{2f_{r,k}(\mathbf{x})} + 2^{m-1} \sigma_{\text{noise}}^2 \\ &= \sum_{k=1}^K \frac{1}{1 + e^{2a_{k,n}^{(\ell)}}} 2^m + 2^{m-1} \sigma_{\text{noise}}^2 \\ &= 2^m \left(\frac{1}{1 + e^{2\xi}} K_n^+ + \frac{1}{2} K_n^0 + \frac{1}{1 + e^{-2\xi}} K_n^- + \frac{1}{2} \sigma_{\text{noise}}^2 \right). \end{aligned}$$

□

APPENDIX B
PROOF OF LEMMA 2

Proof. For a given $\mathbf{V}^{(\ell)}$, $|r_{i(x)}^{(\ell)}|^2$ is an exponential random variable with the mean $\lambda_{i(x)}^{-1} = \sum_{k=1}^K e^{2f_{r,k}(\mathbf{x})} + \sigma_{\text{noise}}^2$ since $r_{i(x)}^{(\ell)}$ is a zero-mean symmetric complex Gaussian distribution in Rayleigh fading channel. Thus, the characteristic function for $|r_{i(x)}^{(\ell)}|^2$ can be calculated as $(1 - jt\lambda_{i(x)}^{-1})^{-1}$, i.e., the Fourier transform of its probability density function (PDF).

The sum of independent random variables is equal to the convolutions of their PDFs. Hence, by using the convolution theorem, the characteristic functions of E_n^+ and E_n^- can be written as the product of the characteristic functions of the corresponding exponential random variables as in $\varphi_n^+(t)$ and $\varphi_n^-(t)$, respectively. Similarly, the characteristic function of $E_n^+ - E_n^-$ is equal to $\varphi_n^+(t)\varphi_n^-(t)^*$.

Based on the inversion formula given in [50], the CDF of $E_n^+ - E_n^-$ can be obtained from its characteristic function as

$$F_{E_n^+ - E_n^-}(x; \mathbf{V}^{(\ell)}) = \frac{1}{2} - \int_{-\infty}^{\infty} \frac{\varphi_n^+(t)\varphi_n^-(t)^*}{2\pi jt} e^{-jtx} dt. \quad (36)$$

□

REFERENCES

- [1] A. Şahin and X. Wang, "Majority vote computation with complementary sequences for distributed UAV guidance," in *Proc. IEEE Military Communications Conference (MILCOM)*, Nov. 2023, pp. 1–6.
- [2] U. Altun, G. Karabulut Kurt, and E. Ozdemir, "The magic of superposition: A survey on simultaneous transmission based wireless systems," *IEEE Access*, vol. 10, pp. 79 760–79 794, 2022.
- [3] A. Şahin and R. Yang, "A survey on over-the-air computation," *IEEE Commun. Surveys Tuts.*, vol. 25, no. 3, pp. 1877–1908, Apr. 2023.
- [4] Z. Chen, E. G. Larsson, C. Fischione, M. Johansson, and Y. Malitsky, "Over-the-air computation for distributed systems: Something old and something new," *IEEE Network*, pp. 1–7, 2023.
- [5] M. Golay, "Complementary series," *IRE Trans. Inf. Theory*, vol. 7, no. 2, pp. 82–87, Apr. 1961.
- [6] B. Nazer and M. Gastpar, "Computation over multiple-access channels," *IEEE Trans. Inf. Theory*, vol. 53, no. 10, pp. 3498–3516, Oct. 2007.
- [7] M. Goldenbaum, H. Boche, and S. Stańczak, "Harnessing interference for analog function computation in wireless sensor networks," *IEEE Trans. Signal Process.*, vol. 61, no. 20, pp. 4893–4906, 2013.
- [8] —, "Nomographic functions: Efficient computation in clustered Gaussian sensor networks," *IEEE Trans. Wireless Commun.*, vol. 14, no. 4, pp. 2093–2105, 2015.
- [9] M. Chen, D. Gündüz, K. Huang, W. Saad, M. Bennis, A. V. Feljan, and H. Vincent Poor, "Distributed learning in wireless networks: Recent progress and future challenges," *IEEE J. Sel. Areas Commun.*, pp. 1–26, 2021.
- [10] A. Şahin, "Distributed learning over a wireless network with non-coherent majority vote computation," *IEEE Trans. Wireless Commun.*, pp. 1–16, 2023.
- [11] G. Zhu, Y. Wang, and K. Huang, "Broadband analog aggregation for low-latency federated edge learning," *IEEE Trans. Wireless Commun.*, vol. 19, no. 1, pp. 491–506, Jan. 2020.
- [12] G. Zhu, Y. Du, D. Gündüz, and K. Huang, "One-bit over-the-air aggregation for communication-efficient federated edge learning: Design and convergence analysis," *IEEE Trans. Wireless Commun.*, vol. 20, no. 3, pp. 2120–2135, Nov. 2021.
- [13] B. McMahan, E. Moore, D. Ramage, S. Hampson, and B. A. y. Arcas, "Communication-Efficient Learning of Deep Networks from Decentralized Data," in *Proc. International Conference on Artificial Intelligence and Statistics (AISTATS)*, A. Singh and J. Zhu, Eds., vol. 54. PMLR, Apr 2017, pp. 1273–1282.
- [14] M. Krouka, A. Elgabli, C. b. Issaid, and M. Bennis, "Communication-efficient split learning based on analog communication and over the air aggregation," in *Proc. IEEE Global Communications Conference (GLOBECOM)*, 2021, pp. 1–6.

- [15] H. Hellström, J. M. B. da Silva Jr., M. M. Amiri, M. Chen, V. Fodor, H. V. Poor, and C. Fischione, "Wireless for machine learning: A survey," *Foundations and Trends in Signal Processing*, vol. 15, no. 4, pp. 290–399, 2022.
- [16] Z. Wang, Y. Zhao, Y. Zhou, Y. Shi, C. Jiang, and K. B. Letaief, "Over-the-air computation: Foundations, technologies, and applications," 2022. [Online]. Available: <https://arxiv.org/abs/2210.10524>
- [17] M. M. Amiri and D. Gündüz, "Federated learning over wireless fading channels," *IEEE Trans. Wireless Commun.*, vol. 19, no. 5, pp. 3546–3557, Feb. 2020.
- [18] W. Guo, R. Li, C. Huang, X. Qin, K. Shen, and W. Zhang, "Joint device selection and power control for wireless federated learning," *IEEE J. Sel. Areas Commun.*, vol. 40, no. 8, pp. 2395–2410, 2022.
- [19] G. Lan, X.-Y. Liu, Y. Zhang, and X. Wang, "Communication-efficient federated learning for resource-constrained edge devices," *IEEE Trans. Machine Learning in Commun. and Netw.*, pp. 1–1, Aug. 2023.
- [20] X. Xie, C. Hua, J. Hong, and Y. Wei, "Joint design of coding and modulation for digital over-the-air computation," 2023. [Online]. Available: <https://arxiv.org/abs/2311.06829>
- [21] A. Şahin, "A demonstration of over-the-air computation for federated edge learning," in *IEEE Globecom Workshops (GC Wkshps)*, 2022, pp. 1821–1827.
- [22] H. Jung and S.-W. Ko, "Performance analysis of UAV-enabled over-the-air computation under imperfect channel estimation," *IEEE Wireless Commun. Lett.*, pp. 1–1, Nov. 2021.
- [23] M. M. Amiri, T. M. Duman, D. Gündüz, S. R. Kulkarni, and H. V. Poor, "Blind federated edge learning," *IEEE Trans. Wireless Commun.*, vol. 20, no. 8, pp. 5129–5143, 2021.
- [24] B. Tegin and T. M. Duman, "Federated learning with over-the-air aggregation over time-varying channels," *IEEE Trans. Wireless Commun.*, pp. 1–14, 2023.
- [25] S. S. M. Hoque and A. Şahin, "Chirp-based majority vote computation for federated edge learning and distributed localization," *IEEE Open Journal of the Communications Society*, pp. 1–1, 2023.
- [26] A. Şahin, "A demonstration of over-the-air-computation for FEEL," in *Proc. IEEE Global Communications Conference Workshops (GLOBECOM WRKSHWP) - Edge Learning over 5G Mobile Networks and Beyond*, Dec. 2022, pp. 1–7.
- [27] A. Gadre, F. Yi, A. Rowe, B. Iannucci, and S. Kumar, "Quick (and dirty) aggregate queries on low-power WANs," in *Proc. ACM/IEEE International Conference on Information Processing in Sensor Networks (IPSN)*, 2020, pp. 277–288.
- [28] A. Şahin and R. Yang, "Over-the-air computation over balanced numerals," in *Proc. IEEE Global Communications Conference Workshops (GLOBECOM WRKSHWP) - Workshop on Wireless Communications for Distributed Intelligence*, Dec. 2022, pp. 1–6.
- [29] G. Mergen and L. Tong, "Type based estimation over multiaccess channels," *IEEE Trans. Signal Process.*, vol. 54, no. 2, pp. 613–626, 2006.
- [30] G. Mergen, V. Naware, and L. Tong, "Asymptotic detection performance of type-based multiple access over multiaccess fading channels," *IEEE Trans. Signal Process.*, vol. 55, no. 3, pp. 1081–1092, 2007.
- [31] M. Goldenbaum and S. Stanczak, "Robust analog function computation via wireless multiple-access channels," *IEEE Trans. Commun.*, vol. 61, no. 9, pp. 3863–3877, 2013.
- [32] —, "On the channel estimation effort for analog computation over wireless multiple-access channels," *IEEE Wireless Commun. Lett.*, vol. 3, no. 3, pp. 261–264, 2014.
- [33] A. Kortke, M. Goldenbaum, and S. Stańczak, "Analog computation over the wireless channel: A proof of concept," in *Proc. IEEE Sensors*, 2014, pp. 1224–1227.
- [34] S. Cai and V. K. N. Lau, "Modulation-free M2M communications for mission-critical applications," *IEEE Transactions on Signal and Information Processing over Networks*, vol. 4, no. 2, pp. 248–263, 2018.
- [35] J. A. Davis and J. Jedwab, "Peak-to-mean power control in OFDM, Golay complementary sequences, and Reed-Muller codes," *IEEE Trans. Inf. Theory*, vol. 45, no. 7, pp. 2397–2417, Nov. 1999.
- [36] P. Park, P. Di Marco, and C. Fischione, "Optimized over-the-air computation for wireless control systems," *IEEE Commun. Lett.*, vol. 26, no. 2, pp. 1–5, 2022.
- [37] J. Lee, Y. Jang, H. Kim, S.-L. Kim, and S.-W. Ko, "Over-the-air consensus for distributed vehicle platooning control (extended version)," 2022. [Online]. Available: <https://arxiv.org/abs/2211.06225>
- [38] X. Zeng, X. Zhang, and F. Wang, "Optimized UAV trajectory and transceiver design for over-the-air computation systems," *IEEE Open Journal of the Computer Society*, pp. 1–9, 2022.
- [39] M. Fu, Y. Zhou, Y. Shi, C. Jiang, and W. Zhang, "UAV-assisted multi-cluster over-the-air computation," *IEEE Trans. Wireless Commun.*, pp. 1–1, 2022.
- [40] A. Şahin and R. Yang, "A generic complementary sequence construction and associated encoder/decoder design," *IEEE Trans. Commun.*, pp. 1–15, 2021.
- [41] Y. M. Mustafah, A. W. Azman, and F. Akbar, "Indoor UAV positioning using stereo vision sensor," *Procedia Engineering*, vol. 41, pp. 575–579, 2012.
- [42] A. Carrio, J. Tordesillas, S. Vemprala, S. Saripalli, P. Campoy, and J. P. How, "Onboard detection and localization of drones using depth maps," *IEEE Access*, vol. 8, pp. 30 480–30 490, 2020.
- [43] X. Chen, T. Chen, H. Sun, Z. S. Wu, and M. Hong, "Distributed training with heterogeneous data: bridging median- and mean-based algorithms," in *Proc. International Conference on Neural Information Processing Systems (NIPS)*. Red Hook, NY, USA: Curran Associates Inc., 2020.
- [44] S. Bouabdallah and R. Siegwart, "Full control of a quadrotor," in *Proc. IEEE/RSJ International Conference on Intelligent Robots and Systems (IROS)*, 2007, pp. 153–158.
- [45] M. G. Parker, K. G. Paterson, and C. Tellambura, "Golay complementary sequences," in *Wiley Encyclopedia of Telecommunications*, 2003.
- [46] E. Dahlman, S. Parkvall, and J. Skold, *5G NR: The Next Generation Wireless Access Technology*, 1st ed. USA: Academic Press, Inc., 2018.
- [47] S.-W. Jeon and B. C. Jung, "Opportunistic function computation for wireless sensor networks," *IEEE Trans. Wireless Commun.*, vol. 15, no. 6, pp. 4045–4059, 2016.
- [48] X. Lv, Y. Niu, and Z. Cao, "Sliding mode control for uncertain 2-D FMII systems under stochastic scheduling," *IEEE Trans. Cyber.*, pp. 1–12, 2023.
- [49] K. J. Åström, *Introduction to stochastic control theory*. Courier Corporation, 2012.
- [50] L. A. Waller, B. W. Turnbull, and J. M. Hardin, "Obtaining distribution functions by numerical inversion of characteristic functions with applications," *The American Statistician*, vol. 49, no. 4, pp. 346–350, 1995.